DFT study of structural and electronic properties of $MoS_{2(1-x)}Se_{2x}$ alloy ($x = 0.25$)

Julia Gusakova,[1] Vasilii Gusakov,[2] and Beng Kang Tay[1,3,a)]
[1]*Novitas Center, Nanyang Technological University, 50 Nanyang Avenue, 639798 Singapore, Singapore*
[2]*Scientific-Practical Materials Research Center, NAS of Belarus, 19 P. Brovki, 220072 Minsk, Belarus*
[3]*CINTRA UMI CNRS/NTU/THALES, 50 Nanyang Drive, 637553 Singapore, Singapore*

(Received 31 October 2017; accepted 25 January 2018; published online 12 February 2018)

First-principles calculations have been performed to study the structural features of the monolayer $MoS_{2(1-x)}Se_{2x}$ ($x = 0.25$) alloy and its electronic properties. We studied the effects of the relative positions of Se atoms in a real monolayer alloy. It was demonstrated that the distribution of the Se atoms between the top and bottom chalcogen planes was most energetically favorable. For a more probable distribution of Se atoms, a $MoS_{2(1-x)}Se_{2x}$ ($x = 0.25$) monolayer alloy is a direct semiconductor with a fundamental band gap equal to 2.35 eV (calculated with the GVJ-2e method). We also evaluated the optical band gap of the alloy at 77 K (1.86 eV) and at room temperature (1.80 eV), which was in good agreement with the experimentally measured band gap of 1.79 eV. *Published by AIP Publishing.* https://doi.org/10.1063/1.5011326

I. INTRODUCTION

The discovery of graphene has opened a wide area of research and application of 2D materials; however, its zero band gap has limited the scope of its applications in electronics.[1] Semiconducting transition metal dichalcogenides (TMDs) represent a class of layered materials. TMD monolayers such as MoS_2, $MoSe_2$, WS_2, and WSe_2 are direct band gap semiconductors (with an optical band gap of 1–2 eV). Owing to a nonzero band gap, rich physics, and promising applications in electronic and optoelectronic devices, transition metal dichalcogenides have attracted much attention.[2–4]

The width of the band gap (fundamental and, as a consequence, optical band gap) is a key parameter that determines the efficiency of many devices such as field effect transistors, photodiodes, phototransistors, and solar cells.[5] So, engineering the band gap of TMD materials with the optimal band gap is the key in fabrication of efficient devices. Because TMD monolayers share a similar atomic structure, it is possible to create an alloy on their base with a tunable band gap. Such a tunable band gap will be defined by the alloy composition.

For TMD materials, depending on the chemical composition of the alloy, two types can be specified. The first type of alloy is characterized by the presence of two different atoms of the transition metal [$Mo_{(1-x)}W_xS_2$ and $Mo_{(1-x)}W_xSe_2$ (Refs. 6 and 7)]. Photoluminescence (PL) characterization of the $Mo_{(1-x)}W_xS_2$ monolayer alloys has shown the continuously tuned emission from 1.82 eV (reached at $x = 0.20$) to 1.99 eV (reached at $x = 1$).[8,9] Moreover, centimeter-scale and high-quality $Mo_{0.5}W_{0.5}Se_2$ alloy films were obtained on both a rigid SiO_2/Si substrate and a flexible polyimide (PI) substrate.[10]

For the second type of alloy, two different chalcogen atoms present in the alloy [$MoS_{2(1-x)}Se_{2x}$ (Refs. 11–15) and $WS_{2(1-x)}Se_{2x}$ (Ref. 6)]. A tunable composition of the $MoS_{2(1-x)}Se_{2x}$ alloy with controlled morphology and a large domain size was obtained with physical vapor deposition (PVD).[16,17] Additionally, ultrathin $MoS_{2(1-x)}Se_{2x}$ alloy nanoflakes, with monolayer or few-layer thicknesses, were prepared through a high-temperature solution method.[18] Li *et al.*[19] reported a simple one-step chemical vapor deposition approach for the simultaneous growth of alloy $MoS_{2x}Se_{2(1-x)}$ triangular nanosheets with complete composition tunability. Further continuous lateral growth of composition-graded bilayer $MoS_{2(1-x)}Se_{2x}$ alloys along single triangular nanosheets was demonstrated by an improved chemical vapor deposition approach.[20] Also, vertical heterostructures, including TMD monolayers and alloys, were synthesized [ex. MoS_2–$MoS_{2(1-x)}Se_{2x}$ (Ref. 21) and $Mo_{1-x}W_xS_2$–WS_2, and $Mo_{1-x}W_xS_2$ alloyed bilayer heterostructures[22]].

The stability and the band gap of MoS_2/$MoSe_2$/$MoTe_2$ alloys have been studied theoretically.[23–25] The optical band gaps of alloys were estimated within the density functional theory (DFT) with Perdew-Burke-Ernzerhof (PBE) approximation for exchange-correlation energy and ranged from 1.65 eV to 2.0 eV.[23] However, it is well known that the PBE generalized gradient approximation (PBE GGA) and GGA+U underestimate the band gap of bulk TMDs by approximately 30%,[26–30] and, for the detailed theoretical study of TMD alloys, a more sophisticated method is needed.

Recently, we proposed the GVJ-2e method developed within the DFT framework for an accurate band gap calculation. The GVJ-2e method is based solely on the total energy computations and is adjustable parameter free. This method demonstrated results with high accuracy and excellent agreement with experiments for a wide range of materials, from bulk semiconductors (ex. Si, C, Ge) to wide gap insulators (ex. Xe, Kr).[31,32] The calculation of the fundamental and optical band gaps of bulk and monolayer TMDs in the GVJ-2e method showed more accurate band gaps than the results obtained with the PBE, hybrid functionals [Heyd-Scuseria-Ernzerhof (HSE)], and GW.[33]

In this paper, we present the theoretical analysis of the energy of formation of a monolayer $MoS_{2(1-x)}Se_{2x}$ alloy ($x = 0.25$) and the microscopic structural stability (different

a)Author to whom correspondence should be addressed: ebktay@ntu.edu.sg

alloy configurations with variation in the positions of substituting atoms of Se). We study electronic properties of the $MoS_{1.5}Se_{0.5}$ alloy, which include the density of states and the fundamental and optical band gap by using the GVJ-2e method. Calculated optical band gaps are compared with experimental PL spectra of $MoS_{2(1-x)}Se_{2x}$ ($x = 0.25$).

II. THEORETICAL BACKGROUND

The fundamental band gap has been calculated in frames of the GVJ-2e method based only on the DFT total energy calculations.[32,33] The final nonlinear equation for the fundamental band gap includes the local density approximation (LDA) band gap and two correction terms when taking into account a nonlocal part of the exchange correlation energy functional and has the form

$$E_g^{(0)} = E_g^{(LDA)} + \frac{1}{2}\Delta_{XC}^{\infty} - \frac{1}{2}E_{(1,0)}^{(\infty,xc)}\left[1 + \exp\left(-\frac{E_g^{(0)}}{E_0}\right)\right], \quad (1)$$

where $E_g^{(0)}$ is the fundamental band gap and E_0 is used only for the dimensionless energy in the exponent (and is determined by the unit of energy, which, in our case, is taken to be equal to $E_0 = 1$ eV). The $E_g^{(LDA)}$ is the band gap defined as the difference between the ionization potential and the electron affinity when two electrons are added or removed from the system and is calculated according to Eq. (2) by using the LDA approximation and referred to as LDA2e. The correction terms are Δ_{XC}^{∞} and $E_{(1,0)}^{(\infty,xc)}$ and could be evaluated from Eqs. (3) and (4). Their precision defines the precision of the calculated band gap

$$E_g = 0.5\left(E_{N+2}^{(0)} + E_{N-2}^{(0)} - 2E_N^{(0)}\right), \quad (2)$$

$$\Delta_{XC}^{\infty} = \left(E_{Z=+2} + E_{Z=-2} - 2E_{Z=0}\right)^{(0)} - \left(E_{Z=+2} + E_{Z=-2} - 2E_{Z=0}\right)^{(LDA)}, \quad (3)$$

$$E_{(1,0)}^{(\infty,xc)} = \left(E_{Z=0}^{(0)} - E_{Z=0}^{(LDA)}\right) - \left(E_{Z=+2}^{(0)} - E_{Z=+2}^{(LDA)}\right). \quad (4)$$

In Eqs. (2)–(4), all the quantities included are the total energies of neutral ($Z = 0$) and charged systems ($Z = +2$ and $Z = -2$). The term $E_{(1,0)}^{(\infty,xc)}$ takes into account a nonlocal part of the exchange-correlation interaction of the pair of electrons at HOMO with the rest of the neutral system.

The final form of Eq. (1) was obtained with the assumption for the limit $\lim_{Eg\to 0} E_{(12,Eg)}^{(\infty,xc)} = E_{(12,0)}^{(\infty,xc)} \approx E_{(1,0)}^{(\infty,xc)}$. The term $E_{(12,Eg)}^{(\infty,xc)}$ describes a nonlocal part of the exchange-correlation energy between the (1) and (2) pairs of electrons in the system with $N + 2$ electrons. The approximation gives good results for band gap computation for such 3D materials as C, Si, Ge, LiF, and BN as well as for wide gap insulators (Xe, Kr).[31] For TMD materials, when a pair of electrons (1) belongs to the *d* orbital (molybdenum), which is more delocalized compared with the *s* and *p* orbitals, we used the following approximation of the limit $\lim_{Eg\to 0} E_{(12,Eg)}^{(\infty,xc)} = E_{(12,0)}^{(\infty,xc)} \approx E_{(1,0)}^{(\infty,xc)} - E_{(2,0)}^{(\infty,xc)}$. In this study, all calculations are made by using a crystal supercell method as implemented in the Quantum Espresso package.[34]

III. RESULTS AND DISCUSSION

MoS_2 and $MoSe_2$ are semiconducting TMDs, which possess the hexagonal symmetry with the space group $P6_3/mmc$. The TMD monolayer (1L) consists of three atomic planes in the configuration when two chalcogen (S or Se) planes sandwich the plane of metal atoms (Mo). Bulk TMD is formed when monolayers are stacked together with weak inter-plane but strong intra-plane interactions.

The $MoS_{2(1-x)}Se_{2x}$ alloy represents a 2D monolayer alloy. It is built from the MoS_2 monolayer, when some of the S atoms are substituted with Se atoms. In a real alloy, for the same concentration *x*, the substituting atoms of Se could occupy different atomic positions in the supercell. We considered the $MoS_{2(1-x)}Se_{2x}$ alloy with the substitution rate $x = 0.25$ (25% of S is replaced with Se), which allows us to study the effect of atomic positions of Se atoms in a real alloy on the structural and electronic properties. Thus, two Se atoms substituted two S atoms in a MoS_2 supercell that contains 12 atoms. There are several possible atomic positions for the Se atoms. Such configurations include the distribution of Se atoms between the top and bottom chalcogen planes (*t1b3, t1b4*, and "stacking" *t1b1*) and the occupation of a single chalcogen plane by Se atoms (*t1t2*, *t1t4*, and *b2b4*). Figure 1 demonstrates all configurations *t1b1*, *t1b3*, *t1b4*, *t1t2*, *t1t4*, *b2b4* of MoS_2 monolayer with two S atoms substituted with Se, which corresponds to the $MoS_{1.5}Se_{0.5}$ monolayer alloy.

Quantum Espresso[34] implementation of the DFT was used for the computation of structural and electronic properties of bulk and monolayer TMDs. We used projector augmented wave (PAW) pseudopotentials and Perdew-Zunger (PZ) LDA[35] and PBE GGA[36] approximations of the exchange-correlation energy. The Brillouin zone was sampled by using the Monkhorst-Pack approach, and $10 \times 10 \times 1$ mesh was used for the monolayer alloy. The kinetic energy cutoff was set to 40 Ry.

For each Se substitution configuration of the $MoS_{1.5}Se_{0.5}$ alloy, first, full relaxation of atomic positions and the lattice parameter (*a*) were performed. The obtained atomic positions

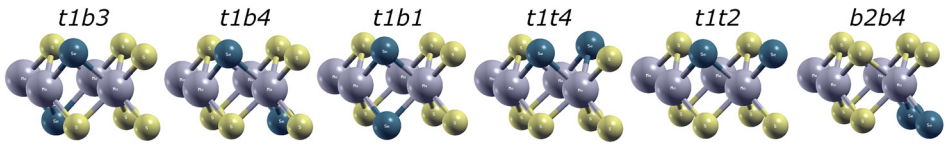

FIG. 1. A $MoS_{1.5}Se_{0.5}$ monolayer alloy with different positions of the Se atoms: top 1 bottom 3 (*t1b3*), top 1 bottom 4 (*t1b4*), top 1 bottom 1 (*t1b1*), top 1 top 4 (*t1t4*), top 1 top 2 (*t1t2*), bottom 2 bottom 4 (*b2b4*). Atoms on the figure: grey, Mo; yellow, S; blue, Se.

and the relaxed lattice parameter were used in all subsequent computations. The fundamental band gaps were calculated by using supercell with 48 atoms.

Table I presents the relaxed lattice parameter of the $MoS_{2(1-x)}Se_{2x}$ ($x = 0.25$) alloy for different positions of Se atoms. The lattice parameter of the relaxed MoS_2 and $MoSe_2$ monolayers differs in approximately 5%. The alloy lattice parameter deviates from the MoS_2 1L lattice parameter by approximately 1%–1.5% for all configurations. Such deviation corresponds to an approximate 11% shift (LDA) of the alloy lattice parameter from the lattice parameter of MoS_2 1L toward the lattice parameter of $MoSe_2$ 1L (17% for PBE). The shift was calculated according to Eq. (6). For the $MoS_{1.5}Se_{0.5}$ alloy monolayer, Boltzmann probability averaging (see Table I) gives lattice parameters 6.311A (PZ LDA) and 6.442A (PBE GGA).

We analyzed the formation energy of a $MoS_{1.5}Se_{0.5}$ supercell with different positions of Se atoms to study the real structure of the alloy. The formation energy of the particular configuration of the alloy is calculated according to the following equation:

$$E_{formation} = E^{MoS_{2(1-x)}Se_{2x}} - (1-x)E^{MoS_2} - xE^{MoSe_2}. \quad (5)$$

Figure 2 presents the formation energy of the $MoS_{1.5}Se_{0.5}$ alloy for different positions of Se atoms. The configurations with a negative formation energy are more stable. The *t1b3* and *t1b4* configurations have the lowest formation energy. These configurations correspond to Se atoms located at the top and bottom chalcogen planes. The *t1b1* configuration (stacking of Se atoms on top of each other) has a higher formation energy but is still negative. This configuration is the most ordered from configurations with Se atoms located in the two planes. The configurations in which both Se atoms are located at the same plane (*t1t4*, *t1t2*, and *b2b4)* have positive formation energy. The latter make them less likely to appear during the synthesis of the $MoS_{1.5}Se_{0.5}$ alloy.

Although it was previously reported that, for the $MoS_{2(1-x)}Se_{2x}$ system, the variation in formation energies is small (few meV), and there is no preference for any particular configuration,[23] we conclude that the configurations *t1b3* and *t1b4* are energetically more favorable. In a real $MoS_{1.5}Se_{0.5}$ alloy, all these configurations will be observed

TABLE I. The relaxed lattice parameter (a) for MoS_2, $MoSe_2$, and $MoS_{1.5}Se_{0.5}$ (for each structural configuration) monolayers and the Boltzmann probabilities of each configuration. All lattice parameters are given in Å for the cell with 12 atoms.

1L	PZ LDA	PBE GGA	Probability
MoS_2	6.282	6.395	
$MoS_{1.5}Se_{0.5}$	6.311	6.442	
t1b3	6.311	6.441	0.236
t1b4	6.311	6.441	0.235
t1b1	6.311	6.441	0.177
t1t4	6.312	6.442	0.120
t1t2	6.312	6.442	0.116
b2b4	6.312	6.445	0.116
$MoSe_2$	6.542	6.669	

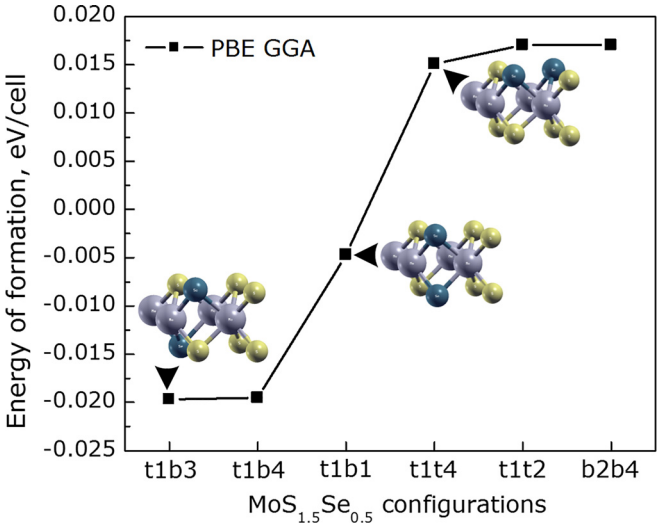

FIG. 2. $MoS_{1.5}Se_{0.5}$ alloy formation energy for different positions of Se atoms (calculated in PBE GGA). Energy values are provided for the cell with 12 atoms. Atoms in the figure: grey, Mo; yellow, S; blue, Se.

with different probabilities. We calculated the partial distribution function for all configurations in a real alloy (see Table I). Most positions of the Se atoms in a real alloy correspond to the configuration with Se atoms distributed between the top and bottom layers.

Recently, we computed the fundamental and optical band gaps of monolayer TMDs (MoS_2, $MoSe_2$, WS_2, and WSe_2) by using the GVJ-2e method.[32] The calculated band gaps were in good agreement with the experimental ones obtained from the scanning tunneling spectroscopy (STS) and PL experiments.

We calculated the fundamental band gaps of the $MoS_{1.5}Se_{0.5}$ alloy with different positions of Se atoms by using the GVJ-2e method according to Eq. (1). Table II presents the calculated GVJ-2e fundamental band gap of the $MoS_{1.5}Se_{0.5}$ alloy. The value of the fundamental band gap not only depends on the substitution rate, but is also sensitive to relative positions of Se atoms in the MoS_2 matrix.

To evaluate the influence of the relative distribution of Se atoms on the fundamental band gap and the lattice parameter, we calculated the shifts according to the following equation:

TABLE II. Theoretical fundamental band gap (GVJ-2e QP) of MoS_2, $MoSe_2$, and $MoS_{1.5}Se_{0.5}$ (for each configuration) monolayers, LDA2e band gaps, and correction terms. Experimental band gaps from STS measurement. All values are in eV.

1L	GVJ-2e QP	Exp.	LDA2e	$E^{(\infty,xc)}_{(1,0)} - E^{(\infty,xc)}_{(2,0)}$	Δ^{∞}_{XC}
MoS_2	2.38	2.40[a]	2.67	0.38	−0.19
$MoS_{1.5}Se_{0.5}$	2.35		2.56	0.26	−0.13
t1b3	2.37		2.57	0.26	−0.13
t1b4	2.37		2.57	0.26	−0.13
t1b1	2.34		2.55	0.25	−0.13
t1t4	2.33		2.53	0.26	−0.13
t1t2	2.33		2.53	0.26	−0.13
b2b4	2.32		2.53	0.27	−0.14
$MoSe_2$	2.12	2.18[b]	2.26	0.17	−0.08

[a]Reference 37.
[b]Room temperature (RT) Ref. 39.

$$shift(E_g) = \frac{E_g^{MoS_{1.5}Se_{0.5}} - E_g^{MoS_2}}{E_g^{MoSe_2} - E_g^{MoS_2}},$$
$$shift(a) = \frac{a^{MoS_{1.5}Se_{0.5}} - a^{MoS_2}}{a^{MoSe_2} - a^{MoS_2}}. \quad (6)$$

Table I highlights that the lattice parameter is almost independent of the Se atom positions for a particular substitution rate, whereas the band gap is very sensitive to the positions of the Se atoms (see Fig. 3). The case in which Se atoms are located on a single plane corresponds to the band gap of approximately 2.32 eV, whereas the distribution of Se atoms between the planes corresponds to band gap values close to 2.37 eV. The configurations in which both Se atoms are concentrated at one plane (*t1t4* and *t1t2*, *b2b4*) have a higher band gap shift toward the $MoSe_2$ band gap. For TMD monolayers, the experimental fundamental band gaps are 2.40 eV and 2.5 eV for MoS_2, and 2.18 eV for $MoSe_2$.[37–39] We obtained the Boltzmann average value of the fundamental band gap of 2.35 eV for the $MoS_{1.5}Se_{0.5}$ alloy by using the calculated probability distribution function (Table II). As expected, the calculated GVJ-2e fundamental band gap of the $MoS_{1.5}Se_{0.5}$ alloy lies in the range between the MoS_2 and $MoSe_2$ band gaps.

We provide the calculation of the fundamental band gap, which should be compared with an experimentally obtained band gap via the STS measurement. Unfortunately, only limited STS measurements are available for pristine TMD monolayers. Usually from an experiment, the optical band gap is available [determined from photoluminescence spectrum (PL)]. It was previously[23] shown that the $MoS_{2(1-x)}Se_{2x}$ alloy band gap was mostly in the red part of a visible spectrum (1.65–2.0 eV). PBE calculations[25] give the value of the $MoS_{1.5}Se_{0.5}$ band gap as 1.63 eV, which differs from the experimentally obtained value of 1.79 eV (Ref. 17) on 0.16 eV (9%).

Therefore, we also estimate the optical band gap for $MoS_{1.5}Se_{0.5}$ alloy at a low temperature by using the $E_g^{PL} = E_g^{QP} - E_{exc.binding}$ equation, where $E_{exc.binding}$ is the exciton binding energy. The theoretical exciton binding energy has been calculated on the basis of the Bethe-Salpeter equation (BSE) theory and equals 0.501 eV and 0.465 eV for MoS_2 and $MoSe_2$ monolayers, respectively.[40] For the alloy $MoS_{1.5}Se_{0.5}$, BSE exciton binding energy is not available. Therefore, in our case, to estimate the exciton binding energy for the $MoS_{1.5}Se_{0.5}$ alloy, we used the following interpolation equation:

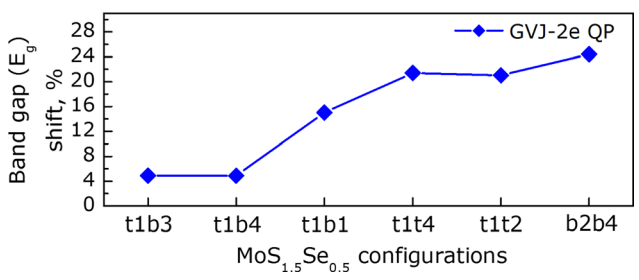

FIG. 3. Calculated shifts of the $MoS_{1.5}Se_{0.5}$ GVJ-2e quasi-particle (QP) band gap from MoS_2 values toward $MoSe_2$.

$$E_{exc.binding}^{alloy} = (1-x)E_{exc.binding}^{MoS_2} + xE_{exc.binding}^{MoSe_2} \quad (7)$$

and obtained $E_{exc.binding}^{MoS_{1.5}Se_{0.5}}$=0.492 eV. Thus, for $MoS_{1.5}Se_{0.5}$ alloy configurations, the optical band gap at low temperature ranges from 1.83 to 1.88 eV.

It was previously demonstrated that PL spectra of MoS_2/$MoSe_2$ depend on the temperature.[41] Namely, the intensity of the PL peak increases both for MoS_2 and $MoSe_2$, and the peak position shifts to lower energy with increasing temperature.

To estimate theoretical PL band gap values at room temperature, we need to estimate the PL band gap shift with temperature. The analytical expression for $E_g(T)$ is lacking, although the origin of band gap temperature dependence is known.[41] We estimate the PL band gap shift with temperature according to the equation $\Delta E_g^T = E_g^{LT} - E_g^{RT}$, which is based on the average experimental values of PL for room and low temperature (77 K) measurements. For MoS_2 and $MoSe_2$ the PL band gap shifts with temperature are $\Delta E_g^T = 0.0475$ eV and $\Delta E_g^T = 0.0802$ eV, respectively. For the $MoS_{1.5}Se_{0.5}$ alloy, the interpolated value of PL band gap shift with temperature equals $\Delta E_g^{T,alloy} = 0.557$ eV, and the band gap at room temperature equals $E_g^{RT} = E_g^{LT} - \Delta E_g^T$. The calculated values of the optical band gap at 0 K (PL LT) and room temperature (PL RT) are presented in Table III.

TABLE III. Calculated GVJ-2e fundamental band gaps for MoS_2, $MoSe_2$, and $MoS_{1.5}Se_{0.5}$ alloy (for each configuration) monolayers. The calculated GVJ-2e optical (PL) band gap for low (PL LT) and room temperature (PL RT) and for Boltzmann averaged values. Experimental values of the PL band gap at RT and LT. Theoretical band gaps from GW, G_0W_0, and HSE are referenced from the literature. Band gap values are in eV.

1L	GVJ-2e QP	GVJ-2e PL LT (PL RT)	Exp. PL LT (PL RT)	GW/G_0W_0 *[HSE]*
MoS_2	2.38	1.88 (RT 1.84)	1.92[a] (RT 1.87[b], 1.89[c], 1.86[d], 1.87[e])	2.97[f]/2.48[g] [2.02[h]]
$MoS_{1.5}Se_{0.5}$	2.35	1.86 (RT 1.80)	RT 1.79[i]	
t1b3	2.37	1.88 (RT 1.82)		
t1b4	2.37	1.88 (RT 1.82)		
t1b1	2.34	1.85 (RT 1.80)		
t1t4	2.33	1.83 (RT 1.78)		
t1t2	2.33	1.84 (RT 1.78)		
b2b4	2.32	1.83 (RT 1.77)		
$MoSe_2$	2.12	1.65 (RT 1.59)	1.62[j], 1.65[k], 1.66[l] (RT 1.54[m], 1.59[n], 1.6[o], 1.52[e]	2.41[f]/2.18[g] [1.72[h]]

[a]77 K Ref. 37.
[b]RT Ref. 42.
[c]RT Ref. 43.
[d]RT Ref. 44.
[e]Our measurement at RT.
[f]GW Ref. 48.
[g]G_0W_0 Ref. 49.
[h]HSE Ref. 24.
[i]RT Ref. 17.
[j]6 K Ref. 45.
[k]76 K Ref. 46.
[l]12 K Ref. 46.
[m]300 K Ref. 45.
[n]RT Ref. 42.
[o]RT Ref. 47.

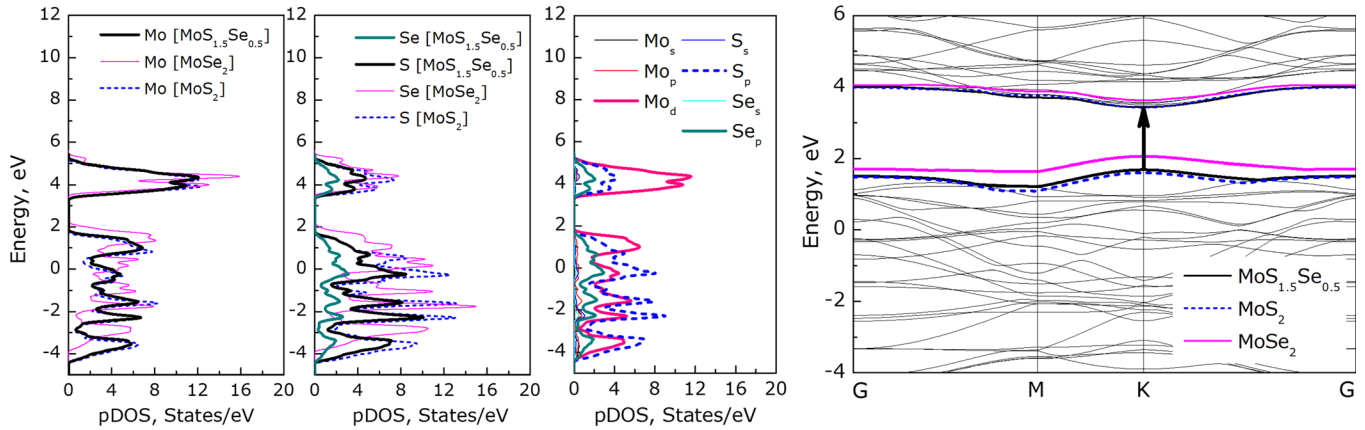

FIG. 4. Comparative projected density of states for Mo, Se, and S atoms in the MoS_2, $MoSe_2$, and $MoS_{1.5}Se_{0.5}$ (*t1b3*) alloy. The projected density of states for Mo, S, and Se in the $MoS_{1.5}Se_{0.5}$ alloy (*t1b3* configuration). A band diagram of the $MoS_{1.5}Se_{0.5}$ alloy (*t1b3*) with top v-band and bottom c-band lines of MoS_2 and $MoSe_2$ (LDA PZ).

We analyzed the projected densities of states (pDOS) of the $MoS_{1.5}Se_{0.5}$ alloy in comparison with MoS_2 and $MoSe_2$ (see Fig. 4). The presence of Se atoms in the MoS_2 matrix affects not only the pDOS of sulphur but also the pDOS of molybdenum. The presence of Se atoms shifts and changes the shape of the Mo pDOS (and the number of states/eV) in the compound compared with the monolayer MoS_2. The $MoS_{1.5}Se_{1.5}$ alloy pDOS is dominated by Mo_d, S_p, and Se_p states.

Figure 5 illustrates a comparison between the calculated band gaps using the GVJ-2e method with the experimental ones. For the $MoS_{1.5}Se_{0.5}$ alloy, only the experimental value for the room temperature PL band gap is available. Averaging the RT values of the band gap over the Boltzmann distribution function for different positions of Se atoms in a real alloy yields $E_g^{RT,alloy} = 1.80$ eV, which is in good agreement with the experimentally obtained 1.79 eV (Ref. 17) [which corresponds to an absolute deviation of 0.01 eV (2%)]. The calculated band diagram of the $MoS_{1.5}Se_{0.5}$ alloy leads to the conclusion that the alloy is a direct band gap semiconductor (see Fig. 4).

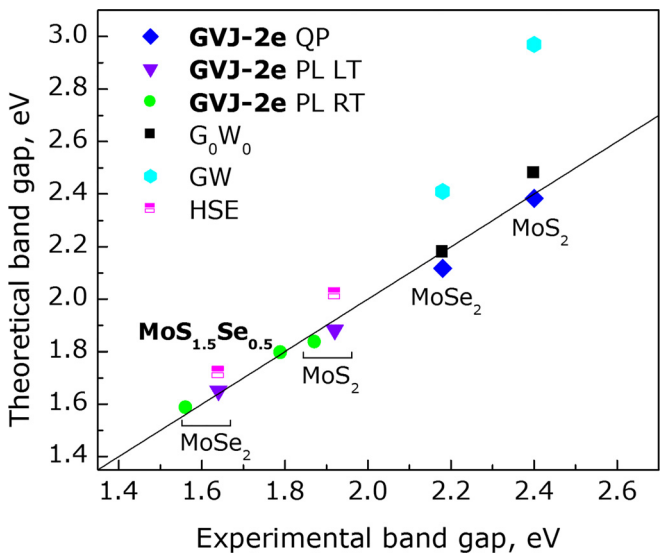

FIG. 5. Comparison of theoretical and experimental band gaps for $MoS_{1.5}Se_{0.5}$, MoS_2, and $MoSe_2$ monolayers: QP, fundamental (quasi-particle) band gap; PL, optical band gap at low (LT) and room (RT) temperatures. Theoretical band gaps include those calculated with the GVJ-2e method (QP, PL LT, PL RT) and values from the literature (GW, G_0W_0, HSE in Table III).

Good agreement between theoretically obtained PL band gaps for low and room temperatures also demonstrates that interpolated values for the exciton binding energy and PL band gap temperature shift could be used to estimate the PL band gap from the calculated fundamental band gap of 2D alloys.

IV. CONCLUSIONS

In this study, we present the first-principles calculations of the structure and electronic properties (fundamental and optical band gap) of 2D alloy $MoS_{1.5}Se_{0.5}$ with the GVJ-2e method.

Analysis of the formation energies of the $MoS_{1.5}Se_{0.5}$ monolayer alloy with different positions of Se atoms shows that alloy configurations with Se atoms distributed between the top and bottom chalcogen planes tend to be more energetically favorable during the synthesis; although the alloy configurations when Se atoms are concentrated at the top or bottom chalcogen plane are less likely to occur.

The calculation shows that the $MoS_{1.5}Se_{0.5}$ monolayer alloy is a direct band gap semiconductor similar to monolayers of MoS_2 and $MoSe_2$. The calculated fundamental band gap equals 2.35 eV and lies between the experimental values of 2.40 eV and 2.5 eV for MoS_2 and 2.18 eV for $MoSe_2$.[37–39] Such an average value corresponds to an approximate 30% shift from an experimental band gap of monolayer MoS_2 toward $MoSe_2$. We also reveal that the fundamental band gap is not only sensitive to the substitution rate but also the relative position of the substituting atoms. We evaluated the exciton binding energy ($E_{exc.binding} = 0.492$ eV) and evaluated the optical band gaps of the $MoS_{1.5}Se_{0.5}$ alloy at low (77 K: $E_g^{PL,LT} = 1.86$ eV) and room ($E_g^{PL,RT} = 1.80$ eV) temperatures. The estimated optical gap at the room temperature of 1.80 eV agrees well with the experimental value of 1.79 eV. This fact confirms that experimentally observed PL transitions correspond to an optical band gap. This study also confirms that

the recently proposed GVJ-2e method could be used for accurate band gap calculations for 2D alloys.

ACKNOWLEDGMENTS

J. Gusakova and B. K. Tay gratefully acknowledge funding support from the Ministry of Education, Singapore (Grant No. MOE2015-T2-2-043).

[1]K. S. Novoselov, A. K. Geim, S. V. Morozov, D. Jiang, Y. Zhang, S. V. Dubonos, I. V. Grigorieva, and A. A. Firsov, Science **306**, 666–669 (2004).
[2]K. S. Novoselov, D. Jiang, F. Schedin, T. J. Booth, V. V. Khotkevich, S. V. Morozov, and A. K. Geim, Proc. Natl. Acad. Sci. U. S. A. **102**, 10451 (2005).
[3]Ch. Tan, X. Cao, X.-J. Wu, Q. He, J. Yang, X. Zhang, J. Chen, W. Zhao, S. Han, G.-H. Nam, M. Sindoro, and H. Zhang, Chem. Rev. **117**, 6225–6331 (2017).
[4]X. Li, L. Tao, Z. Chen, H. Fang, X. Li, X. Wang, J.-B. Xu, and H. Zhu, Appl. Phys. Rev. **4**, 021306 (2017).
[5]T. Jin, J. Kang, E. S. Kim, S. Lee, and C. Lee, J. Appl. Phys. **114**, 164509 (2013).
[6]Y. Sun, K. Fujisawa, Z. Lin, Y. Lei, J. S. Mondschein, M. Terrones, and R. E. Schaak, J. Am. Chem. Soc. **139**, 11096–11105 (2017).
[7]X. Li, A. A. Puretzky, X. Sang, S. KC, M. Tian, F. Ceballos, M. Mahjouri-Samani, K. Wang, R. R. Unocic, H. Zhao, G. Duscher, V. R. Cooper, C. M. Rouleau, D. B. Geohegan, and K. Xiao, Adv. Funct. Mater. **27**, 1603850 (2017).
[8]D. Dumcenco, H. Kobayashi, Z. Liu, Y. S. Huang, and K. Suenaga, Nat. Commun. **4**, 1351 (2013).
[9]Y. F. Chen, J. Y. Xi, D. O. Dumcenco, Z. Liu, K. Suenaga, D. Wang, Z. G. Shuai, Y. S. Huang, and L. M. Xie, ACS Nano **7**, 4610–4616 (2013).
[10]Z. Zheng, J. Yao, and G. Yang, ACS Appl. Mater. Interfaces **9**, 14920–14928 (2017).
[11]J. Mann, Q. Ma, P. M. Odenthal, M. Isarraraz, D. Le, E. Preciado, D. Barroso, K. Yamaguchi, G. von Son Palacio, A. Nguyen, T. Tran, M. Wurch, A. Nguyen, V. Klee, S. Bobek, D. Sun, T. F. Heinz, T. S. Rahman, R. Kawakami, and L. Bartels, Adv. Mater. **26**, 1399–1404 (2014).
[12]Y. Gong, Z. Liu, A. R. Lupini, G. Shi, J. Lin, S. Najmaei, Z. Lin, A. L. Elías, A. Berkdemir, G. You, H. Terrones, M. Terrones, R. Vajtai, S. T. Pantelides, S. J. Pennycook, J. Lou, W. Zhou, and P. M. Ajayan, Nano Lett. **14**, 442–449 (2014).
[13]J. Jadczak, A. Delgado, L. Bryja, Y. S. Huang, and P. Hawrylak, Phys. Rev. B **95**, 195427 (2017).
[14]S. Umrao, J. Jeon, S. M. Jeon, Y. J. Choi, and S. Lee, Nanoscale **9**, 594–603 (2017).
[15]J. Kang, S. Tongay, J. Li, and J. Wu, J. Appl. Phys. **113**, 143703 (2013).
[16]Q. Feng, N. Mao, J. Wu, H. Xu, C. Wang, J. Zhang, and L. Xie, ACS Nano **9**(7), 7450–7455 (2015).
[17]Q. Feng, Y. Zhu, J. Hong, M. Zhang, W. Duan, N. Mao, J. Wu, H. Xu, F. Dong, F. Lin, C. Jin, C. Wang, J. Zhang, and L. Xie, Adv. Mater. **26**, 2648–2653 (2014).
[18]Q. Gong, L. Cheng, C. Liu, M. Zhang, Q. Feng, H. Ye, M. Zeng, L. Xie, Z. Liu, and Y. Li, ACS Catal. **5**, 2213–2219 (2015).
[19]H. Li, X. Duan, X. Wu, X. Zhuang, H. Zhou, Q. Zhang, X. Zhu, W. Hu, P. Ren, P. Guo, L. Ma, X. Fan, X. Wang, J. Xu, A. Pan, and X. Duan, J. Am. Chem. Soc. **136**, 3756–3759 (2014).
[20]H. Li, Q. Zhang, X. Duan, X. Wu, X. Fan, X. Zhu, X. Zhuang, W. Hu, H. Zhou, A. Pan, and X. Duan, J. Am. Chem. Soc. **137**, 5284–5287 (2015).
[21]H. Li, X. Wu, H. Liu, B. Zheng, Q. Zhang, X. Zhu, Z. Wei, X. Zhuang, H. Zhou, W. Tang, X. Duan, and A. Pan, ACS Nano **11**, 961–967 (2017).
[22]F. Chen, L. Wang, X. Ji, and Q. Zhang, ACS Appl. Mater. Interfaces **9**, 30821–30831 (2017).
[23]H.-P. Komsa and A. V. Krasheninnikov, J. Phys. Chem. Lett. **3**, 3652–3656 (2012).
[24]J. Kang, S. Tongay, J. Zhou, J. Li, and J. Wu, Appl. Phys. Lett. **102**, 012111 (2013).
[25]B. Rajbanshi, S. Sarkar, and P. Sarkar, Phys. Chem. Chem. Phys. **17**, 26166–26174 (2015).
[26]H. Jiang, J. Phys. Chem. C **116**, 7664 (2012).
[27]W. Li, Ch. F. J. Walther, A. Kuc, and T. Heine, J. Chem. Theory Comput. **9**, 2950 (2013).
[28]A. Kuc, N. Zibouche, and T. Heine, Phys. Rev. B **83**, 245213 (2011).
[29]S. Kumar and U. Schwingenschlögl, Chem. Mater. **27**, 1278 (2015).
[30]N. Zibouche, A. Kuc, J. Musfeldt, and T. Heine, Ann. Phys. **526**, 395 (2014).
[31]J. Gusakova, B. K. Tay, and V. Gusakov, "Efficient DFT method for calculating band gap and deep levels in semiconductors," in 28th ICDS Conference, Helsinki, Finland (2015).
[32]J. Gusakova, B. K. Tay, and V. Gusakov, Phys. Status Solidi A **213**(11), 2834–2837 (2016).
[33]J. Gusakova, X. Wang, L. L. Shiau, A. Krivosheeva, V. Shaposhnikov, V. Borisenko, V. Gusakov, and B. K. Tay, Phys. Status Solidi A **214**, 1700218 (2017).
[34]P. Giannozzi, S. Baroni, N. Bonini, M. Calandra, R. Car, C. Cavazzoni, D. Ceresoli, G. L. Chiarotti, M. Cococcioni, I. Dabo, A. Dal Corso, S. de Gironcoli, S. Fabris, G. Fratesi, R. Gebauer, U. Gerstmann, C. Gougoussis, A. Kokalj, M. Lazzeri, L. Martin-Samos, N. Marzari, F. Mauri, R. Mazzarello, S. Paolini, A. Pasquarello, L. Paulatto, C. Sbraccia, S. Scandolo, G. Sclauzero, A. P. Seitsonen, A. Smogunov, P. Umari, and R. M. Wentzcovitch, J. Phys.: Condens. Matter **21**, 395502 (2009).
[35]J. P. Perdew and A. Zunger, Phys. Rev. B **23**, 5048 (1981).
[36]J. P. Perdew, K. Burke, and M. Ernzerhof, Phys. Rev. Lett. **77**, 3865 (1996).
[37]Y. L. Huang, Y. Chen, W. Zhang, S. Y. Quek, C.-H. Chen, L.-J. Li, W.-T. Hsu, W.-H. Chang, Y. J. Zheng, W. Chen, and A. T. S. Wee, Nat. Commun. **6**, 6298 (2015).
[38]A. R. Klots, A. K. M. Newaz, B. Wang, D. Prasai, H. Krzyzanowska, J. Lin, D. Caudel, N. J. Ghimire, J. Yan, B. L. Ivanov, K. A. Velizhanin, A. Burger, D. G. Mandrus, N. H. Tolk, S. T. Pantelides, and K. I. Bolotin, Sci. Rep. **4**, 6608 (2014).
[39]M. M. Ugeda, A. J. Bradley, S.-F. Shi, F. H. da Jornada, Y. Zhang, D. Y. Qiu, W. Ruan, S.-K. Mo, Z. Hussain, Z.-X. Shen, F. Wang, S. G. Louie, and M. F. Crommie, Nat. Mater. **13**, 1091 (2014).
[40]T. Olsen, S. Latini, F. Rasmussen, and K. S. Thygesen, Phys. Rev. Lett. **116**, 056401 (2016).
[41]S. Tongay, J. Zhou, C. Ataca, K. Lo, T. S. Matthews, J. Li, J. C. Grossman, and J. Wu, Nano Lett. **12**, 5576 (2012).
[42]J. O. Island, A. Kuc, E. H. Diependaal, R. Bratschitsch, H. S. J. van der Zant, T. Heine, and A. Castellanos-Gomez, Nanoscale **8**, 2589 (2016).
[43]K. F. Mak, C. Lee, J. Hone, J. Shan, and T. F. Heinz, Phys. Rev. Lett. **105**, 136805 (2010).
[44]A. Steinhoff, J.-H. Kim, F. Jahnke, M. Rösner, D.-S. Kim, C. Lee, G. H. Han, M. S. Jeong, T. O. Wehling, and C. Gies, Nano Lett. **15**(10), 6841–6847 (2015).
[45]F. Withers, O. Del Pozo-Zamudio, S. Schwarz, S. Dufferwiel, P. M. Walker, T. Godde, A. P. Rooney, A. Gholinia, C. R. Woods, P. Blake, S. J. Haigh, K. Watanabe, T. Taniguchi, I. L. Aleiner, A. K. Geim, V. I. Fal'ko, A. I. Tartakovskii, and K. S. Novoselov, Nano Lett. **15**, 8223–8228 (2015).
[46]T. Godde, D. Schmidt, J. Schmutzler, M. Aßmann, J. Debus, F. Withers, E. M. Alexeev, O. Del Pozo-Zamudio, O. V. Skrypka, K. S. Novoselov, M. Bayer, and A. I. Tartakovskii, Phys. Rev. B **94**, 165301 (2016).
[47]G. W. Shim, K. Yoo, S.-B. Seo, J. Shin, D. Y. Jung, I.-S. Kang, C. W. Ahn, B. J. Cho, and S.-Y. Choi, ACS Nano **8**(7), 6655–6662 (2014).
[48]H.-P. Komsa and A. V. Krasheninnikov, Phys. Rev. B **86**, 241201(R) (2012).
[49]F. A. Rasmussen and K. S. Thygesen, J. Phys. Chem. C **119**, 13169–13183 (2015).